Introducing the Next-generation Advanced Baseline Imager (ABI) on Geostationary Operational Environmental Satellites (GOES)-R

Timothy J. Schmit
NOAA/NESDIS, Office of Research and Applications, Advanced Satellite Products Team (ASPT), Madison, WI 53706

Mathew M. Gunshor
Cooperative Institute for Meteorological Satellite Studies (CIMSS), University of Wisconsin-Madison

W. Paul Menzel
NOAA/NESDIS, Office of Research and Applications, Madison, WI 53706

Jun Li
Cooperative Institute for Meteorological Satellite Studies (CIMSS), University of Wisconsin-Madison

Scott Bachmeier
Cooperative Institute for Meteorological Satellite Studies (CIMSS), University of Wisconsin-Madison

James J. Gurka
NOAA/NESDIS, Office of Systems Development, Silver Spring, Maryland

To be Submitted to: *Bull. of the AMS*

Version date: May 6, 2004

Corresponding author address: Timothy J. Schmit, 1225 West Dayton Street, Madison, WI 53706; email: Tim.J.Schmit@noaa.gov. Telephone: (608) 263-0291.

ABSTRACT

A new era in environmental remote sensing has begun as the Advanced Baseline Imager (ABI) is being designed for future Geostationary Operational Environmental Satellites (GOES) starting with GOES-R (scheduled for launch in 2012). As with the current GOES Imager, the ABI will be used for a wide range of qualitative and quantitative weather, oceanographic, climate and environmental applications. The ABI will improve over the existing GOES Imager with more spectral bands, faster imaging (and more geographical areas scanned), higher spatial resolution, nominally improving from 4 to 2 km for the infrared bands and 1 to 0.5 km for the 0.64 μm visible band. There will be an increase of the coverage rate leading to full disk scans at least every 15 minutes. The ABI expands from five spectral bands on the current GOES imagers to 16 spectral bands in the visible, near-infrared and infrared spectral regions. The purpose of these bands is summarized. Every product that is being produced from the current GOES Imager will be improved with data from the ABI, plus there will be a host of new products possible. For example, today's GOES Imagers have no sensitivity to SO_2, while the ABI will be able to detect some upper-level SO_2 plumes. Other new products include monitoring plant health on a diurnal time scale, cloud-top phase and particle size information, and much improved aerosol and smoke detection for air quality monitoring and forecasts. While the ABI represents an exciting expansion in geostationary remote sensing capabilities, it will not be operating alone. Where appropriate, products will be produced in concert with the GOES-R high-spectral resolution sounder, part of the Hyperspectral Environmental Suite (HES). Several products can be improved when using high spatial resolution imager data with co-located high-spectral resolution measurements.

1. INTRODUCTION

The Advanced Baseline Imager (ABI) is the planned Imager on the Geostationary Operational Environmental Satellite (GOES) series, starting a new era in approximately 2012 with GOES-R (Gurka and Dittburner, 2001). Like the current GOES Imager, the ABI will be used for a wide range of qualitative and quantitative weather, climate and environmental applications. The ABI will improve over the existing GOES Imager with more spectral bands, higher spatial resolution, faster imaging, and broader spectral coverage. The ABI spatial resolution will be nominally 2 km for the infrared bands and 1 to 0.5 km for the 0.64 μm visible band. There will be a five-fold increase in the coverage rate. The ABI will scan the full disk at least every fifteen minutes, plus CONUS (CONtinental United States) images every five minutes plus a selectable 1000 km by 1000 km area image. A 5 minute full disk scan mode is also planned. The ABI expands the spectral band number to 16; five are similar to the 0.6, 4, 11, and 12 μm windows and the 6.5 μm water vapor band on the current GOES-8/11 Imagers. Another is similar to the 13.3 μm on the GOES-12/N/O/P imagers (Hillger et al. 2003; Schmit et al. 2001). For more information on the current GOES Imager and Sounder see Menzel and Purdom (1994), Ellrod et al. (1998) or Schmit et al. (2002). Additional bands on the ABI are a visible band at 0.47 μm for aerosol detection and visibility estimation; a band at 0.86 μm for the detection of aerosols and health of the vegetation/burn scars; a near-infrared band at 1.38 μm to detect very thin cirrus clouds; a snow/cloud-discriminating 1.6 μm band; the 2.26 μm will be used to estimate aerosol and cloud particle size, vegetation and cloud properties/screening, hot spot detection, moisture determinations and snow detection; mid-tropospheric bands centered near the 7.0 and 7.34 μm water vapor bands to track atmospheric motions and detect upper-level Sulfur Dioxide (SO_2); an 8.5 μm band to detect volcanic dust clouds containing sulfuric acid aerosols and cloud phase; the 9.6 μm band for monitoring atmospheric total column ozone and upper-level dynamics; and the 10.35 μm band to derive low-level moisture and cloud particle size.

While the ABI represents an exciting expansion in geostationary remote sensing capabilities, it will not be operating alone. Where appropriate, the ABI will be used in concert with the GOES-R high-spectral resolution sounder, the HES (Hyperspectral Environmental Suite). The ABI high spatial resolution data will help flag sub-pixel clouds in the HES infrared measurements (Li et al, 2004), while the high spectral resolution HES measurements will offer an improved surface emissivity for determining skin temperatures from ABI data as well improved cloud heights estimates, especially for thin clouds. A Cost Benefit Analysis study showed combined annual marginal economic benefits from ABI and HES are greater than $500 M annually (in 2002 dollars). This is projected when considering a few key representative economic sectors (agriculture, aviation, electric power and natural gas generation, recreational boating, and trucking). Every product from the current GOES Imager will be improved with data from the ABI (and HES), and a host of new products will be possible. Monitoring of: hurricane intensities, land and sea temperatures, cloud-top heights/temperatures, fires and hot spots, insolation, precipitation and fog will be improved. In addition the ABI will be able to detect some upper-level SO_2 clouds, monitor plant health on a diurnal time scale, infer cloud-top phase and particle size information, and improve aerosol/smoke detection.

The various spectral bands on the GOES-R ABI are simulated in two ways. The first method is to use forward model calculations for various atmospheres to show weighting functions and/or calculated brightness temperatures (BT) for comparison with similar bands on other instruments such as the current GOES Imagers. Realistic simulations of cloudy radiances can be time consuming and required advanced forward models. The second method is to use existing satellite data to simulate the ABI spectral bands. One option is to use broadband imagers like the MODIS (MODerate-resolution Imaging Spectroradiometer) and resample the data to the ABI spatial resolutions. Another option is to use high-spectral resolution data convolved with simulated ABI Spectral Response Functions (SRF); these include AIRS (Atmospheric InfraRed Sounder), NAST-I (NPOESS Atmospheric Sounder Testbed-Interferometer), and AVIRIS (Airborne Visible InfraRed Imaging Spectrometer) (Aumann et al., 2003, Vane 1987). Each method has strengths and weaknesses and both methods are used in this paper to demonstrate future ABI capabilities.

The six proposed visible/near infrared bands are shown in Figure 1 with representative high spectral plots that correspond to snow and vegetation. Some of the improved or new products possible with these visible/near infrared bands include detection of haze, clouds, surface vegetation, cirrus, snow cover and aerosol particle sizes. Vegetation

estimates can be obtained by comparing the two bands on either side of the 0.72 μm transition region, while snow can be determined by comparing two visible bands on either side of the transition for snow reflectance at approximately 1.4 μm. Figure 2 shows the ten proposed bands in the infrared portion of the spectra. Note the improved spectral coverage of the ABI compared to either the GOES-8/11 or GOES-12/P imagers. The region of the atmosphere where the ABI infrared (IR) bands receive their signal is shown in Figure 3. These weighting functions, for the standard atmosphere at a satellite view angle of 40 degrees, show the peak of the ozone-sensitive band is furthest aloft, followed by the three water vapor weighting functions, and then the CO_2-sensitive band and finally the various surface viewing bands. Simulated ABI SRF were used to build the fast radiative transfer model required for these calculations.

Select new and improved products possible with the GOES ABI are summarized in Section 2. Section 3 briefly describes each of the bands on the ABI. A discussion of the heritage of each spectral band is given in Section 4. Finally, a summary is presented in Section 5.

2. PRODUCTS

Examples of ABI products are presented in the broad categories of imagery/radiances, atmospheric products, oceanographic products, land products, and hazard detection.

2.1 Imagery/Radiances

There are numerous uses for each of the current bands on the GOES Imager when displayed as a time-series of images. This will also be the case for each of the ABI bands. For example, the current GOES Imager "water vapor" band 3 (6.5/6.7 μm) has many applications, ranging from estimating upper level moisture (Soden et al., 1993; Moody et al., 1999) to defining upper-level jetstreaks (Weldon et al., 1991). Additional information will be gleamed by differencing bands or applying principle component analysis on the imagery (Hillger, 1996). The difference between the 11 and 12 μm BTs, known as the split window, helps detect dust, volcanic ash plumes, low-level moisture, skin temperature and aids in distinguishing between cloud types and biomass burning aerosols (Ackerman, 1996; Ackerman et al., 1992; Moeller et al., 1996; Prata, 1989, Barton et al., 1992; Hayden et al., 1996; Prins et al., 1998). Outflow boundaries have also been observed (Dostalek et al. 1997). The difference between the 6.7 μm and the 11 μm bands has been shown to be correlated to convection (Mosher, 2001).

Spatially averaged clear-sky BTs are produced from the imagers for inclusion in numerical models. For example, the direct assimilation of water vapor (WV) clear-sky brightness temperatures (CSBT) from Meteosat-7 became operational at ECMWF (European Centre for Medium-range Weather Forecasts) in April 2002 using the four-dimensional variational assimilation (4DVAR) system. ECMWF is also assimilating the hourly water vapor band from the Imagers on GOES-9, -10 and –12 (Szyndel et al. 2003). The Canadian Meteorological Centre also assimilates radiances from the GOES Imagers, including surface viewing bands (Garand 2003). The GOES CSBT product will be improved for the ABI, in part due to a superior cloud mask possible with the additional ABI bands and the higher signal-to-noise ratio. Most of the ABI IR bands have a specified noise of 0.1K at a reference temperature of 300K; the 13.3 μm band has at noise specification of 0.3K at 300 K. The ABI will also have more bands for assimilation in numerical models, representing different layers of the earth-atmosphere system.

ABI radiances will also be used to derive a cloud mask that separates clear from cloudy sky radiances. The algorithm will start with the spectral and spatial tests demonstrated in the MODIS cloud mask (Ackerman et al. 1998) and supplement these with temporal consistency tests.

2.2 Atmospheric Products

Cloud products generated via the CO_2 absorption technique have been demonstrated from instruments on both geostationary and polar-orbiting platforms (Wylie and Wang, 1997; Schreiner et al., 1993; Wylie et al., 1994; Wylie and Menzel, 1999; Frey et al., 1999; Schreiner et al., 2001). Cloud products derived from the GOES Sounder have been used to initialize numerical models (Kim et al., 2000; Bayler et al., 2001). Improved products from the GOES ABI will include cloud top pressure/height, effective cloud amount (representative of cloud optical thickness), and cloud top temperature. Also, several of the bands new on the ABI will allow cloud-top particle size and cloud phase to be determined. As with MODIS data (Platnick et al., 2003), cloud and surface classifications will be generated (Li et al. 2003). ABI cloud products will also be computed in conjunction with information from the Hyperspectral Environmental Suite (HES) (Li et al., 2002).

Rainfall estimation techniques rely on the infrared window, for example the auto-estimator (Vicente et al., 1998), or additional, such as the GOES Multispectral Rainfall Algorithm (GMSRA) (Ba et al., 2001). These satellite rainfall estimations will be improved with the ABI higher spatial resolution (better depiction of cold cores), more frequent images (improved cell growth information), improved cloud heights (with multiple bands and HES), introduction of cloud phase (new ABI bands), better signal-to-noise ratios, and better navigation/registration. For example, the time tendency of BTs can be used to help categorize cell growth.

The tracking atmospheric features (Velden et al., 1997) will be enhanced using the ABI data with the higher spatial resolution (better edge detection), more frequent images (offers different time intervals), better cloud height detection (with multiple bands), new bands (0.86, 1.38 μm), better signal-to-noise ratio, and better image navigation/registration. Currently, the atmospheric motion height assignment is one of the greatest sources of error (Nieman et al., 1993). These errors will be reduced with data from the ABI and HES.

The GOES Imager is used to determine hurricane location and intensity (Velden et al., 1998a and 1998b; Goerss et al., 1998; Bosart et al. 2000). The Objective Dvorak Technique (ODT) relies on the longwave infrared window band to monitor the strength of tropical cyclones (Velden et al., 1998a). This product will be improved due to improved temporal and spatial resolutions; it is estimated that the spatial improvements alone may lead to ODT improvements of up to half a category due to increased ability to detect warming in the eye and detailed structure in the cold eyewall region (DeMaria, personal communication). The ABI, in conjunction with the HES, will also allow investigation of multi-spectral approaches for estimating hurricane intensity.

2.3 Oceanographic Products

The GOES platform allows frequent looks at a given area with the same viewing angle. This enables improved spatial and temporal coverage of Sea Surface Temperature (SST) from the GOES Imager (Wu et al., 1999; Legeckis, 2002). The GOES SST has applications ranging from weather forecasting to fisheries management (Seki et al., 2001). Time animation of GOES SST fields (to deduce regions of stronger currents) have also been used for safe oil and gas operations in the Gulf of Mexico (Walker et al., 2003). ABI SST will be improved through higher spatial resolution, more frequent images, more spectral bands, better atmospheric correction (in part with data from the HES), better cloud and aerosol detection, and less instrument noise.

Suspended sediments in coastal waters can be detected with a 0.86 μm band (Aquirre-Gomez, 2000). While these estimates would not be as fine as that from the visible/near-infrared HES-Coastal Waters (CW), the ABI-based estimate could be used to help determine either where the HES-CW should scan or possibly monitor changes between HES-CW observations.

2.4 Hazards

The detection of volcanic ash plumes is important for aviation (Casadevall et al., 1992; Davies and Rose, 1998, Hillger and Clark, 2002; Ellrod, 2001). The ABI volcanic ash detection will depend on 12 μm data (Schmit et al. 2001), plus

7.34 and 8.5 μm data. The ABI water vapor bands have been shifted to detect upper-level SO_2, as well as the mid-level water vapor. Forward calculations with the PFAAST (Pressure-layer Fast Algorithm for Atmospheric Transmittance) (Hannon et al, 1996) radiative transfer model (Figure 4) show the sensitivity of the 7.34 and 8.5 μm bands to SO_2 for the U.S. standard atmosphere. If the vertical and spatial extents of the plume are sufficient, the ABI should be able to detect medium to large SO_2 amounts (greater than 100 Dobson Units (DU)), but not small amounts (less than 50 DU). High-spectral resolution measurements, if they include the 7 μm region, should have more sensitivity than broadband radiometers for detecting SO_2 because individual absorption features can be used. ABI bands, simulated from AIRS data, show the potential for depicting upper-level SO_2 (Figure 5). This case is from July 13, 2003.

Detection of dust will be also be improved with data from the ABI. For example, the 8.5, 11, and 12 μm bands have revealed sandstorms (Gu et al., 2003).

The bispectral 4 and 11 μm technique for fog detection (Ellrod et al., 1998) is based on difference essimivities of fog in the longwave and shortwave IR windows. Using simulated ABI data (derived from 1 km MODIS data), it has been shown that the fog detection of ABI is an improvement over the current GOES Imager. The ABI offers both improved spatial and temporal measurements.

An experimental GOES product highlights areas of supercooled water clouds that could produce aircraft icing (Ellrod, 1996) using split window (11 μm band minus 12 μm band) BT differences greater than 2 K to flag thin cirrus. The addition of the 1.6 and 8.5 μm bands will improve this product.

The 0.47 μm band will also detect daytime smoke/aerosols and hence air quality at high temporal resolutions. Due to the episodic nature of these events, the improved temporal scans from the geostationary perspective are needed.

2.5 Surface Products

Detection of active fires with the 3.9 and 11 μm bands (Prins et al. 1998) will be improved with the ABI improved spatial and temporal resolutions, along with the hotter maximum temperature detectable in these bands. The geostationary perspective allows for the diurnal monitoring of fires. Fire location and characteristic will also be used to improve air quality/visibility forecasts.

A near infrared (NIR) channel at 0.86 μm will enable monitoring of vegetation trends and health, similar to the global AVHRR (Advanced Very High Resolution Radiometer) vegetation monitoring (Kogan 1990, Tarpley, et al, 1984). The ABI will be able to monitor localized vegetation stress, help to estimate fire danger, and detect fire burn scars. ABI will present an improved NDVI (Normalized Difference Vegetation Index) product in smoky regions using the 2.26 μm band (Karnieli et al. 2001). The 2.26 μm band is much less sensitive to smoke than the 0.64 μm band since the presence of smoke back-scatters more solar radiation at shorter wavelengths. Using MODIS data, Figure 6a shows an NDVI calculated with the 2.1 μm band in a smoke-free region that is highly correlated (correlation coefficient of 0.94) to the traditional NDVI product, but less correlated (correlation coefficient of 0.55) in regions of smoke (Figure 6b). Replacing shorter wavelengths, such as 0.64 um, with a longer wavelength, such as 2.1 or 2.26 μm, results in an NDVI that is much less sensitive to smoke. Of course a multi-spectral approach may be optimal.

3. INDIVIDUAL BANDS OF THE PROPOSED ABI

Of the 16 ABI channels, three will be in the visible, three will be in the near infrared (NIR), and ten will be in the infrared (IR) regions of the electromagnetic spectrum. Information about the spectral bands of the current GOES Imagers is given in Table 1, including approximate spectral widths, central wavelength, and approximate sub-satellite point resolutions. The GOES Imager oversamples in the east-west by a factor of 1.7. The 13.3 μm will be 4 km beginning on GOES-O. Table 2 lists the bands of the ABI. These bands will be used to support weather nowcasting, numerical weather prediction, oceanography, hydrology, land surface, natural hazards and climate (NOAA NESDIS, 2001).

3.1 Visible bands

The utility of a band centered at 0.47 μm is well established from many satellites in low-earth orbit, such as MODIS on NASA's Terra and Aqua platforms. A geosynchronous platform is complementary to the polar orbiters, providing unique diurnal data at mesoscale resolution. The 0.47 μm band will provide nearly continuous observations of clouds, dust, haze, and smoke. Measurements of Aerosol Optical Depths (AOD) will help monitoring and forecasting air quality. The geostationary satellite perspective enables tracking AOD transport (Kittaka et al, 2004). Finally, a blue band (0.47 μm), a green band (which will need to be simulated from other bands on the ABI), and a red band (0.64 μm) bands can be combined to provide "natural color" imagery of the earth, ocean, and atmospheric system. The "blue" channel will be valuable for aviation applications via estimates of slant-range visibility. The shorter wavelengths (blue) are scattered more in haze and air particles than the longer wavelengths (red). The 0.47 μm band will also have potential applications for air pollution studies, and for improving numerous products that rely on obtaining clear sky radiances (i.e. land and sea surface products).

The ABI 0.64 μm has many uses, including the diurnal aspects of daytime clouds, fog detection and solar insolation (Diak et al., 1998). The 0.64 μm visible band is also used for: daytime snow and ice cover; detection of severe weather; low-level cloud drift winds; fog; smoke; volcanic ash; hurricane analysis; and winter storm analysis. The current GOES Imager has demonstrated many of these applications with a similar band.

3.2 Near-Infrared bands

Along with the 0.64 μm band, the 0.86 μm band is used for detecting daytime clouds, NDVI, fog, and aerosols. This band can help in determining vegetation amount and aerosol locations, and can be used for ocean and land studies. The GOES perspective is well suited for sensing diurnal changes. This may have implications in forecasting forest re-growth patterns. The current GOES visible channel (0.52 - 0.72 μm) does not delineate the burn scars. Low-level winds may be derived from time sequences of 0.86 μm images, especially over the water.

The 1.38 μm band helps to detect very thin cirrus clouds during the day (Gao et al, 2002). This band centered in a strong water vapor absorption spectral region (Figure 1) does not sense the lower troposphere and thus provides excellent daytime sensitivity to very thin cirrus. Surface or lower troposphere cloud reflection is attenuated (for most atmospheres). Improved contrail detection possible with this band is important when estimating many surface parameters. When the Total Precipitable Water (TPW) is less than approximately 10 mm, reflectance from the surface minimizes the benefits of this band for thin cirrus detection (Sieglaff et al., 2003).

During the day, the 1.6 μm band is used for cloud/snow/ice discrimination, total cloud cover estimation, cloud-top phase (Hutchison 1999), and smoke detection from low-burn-rate fires. The daytime water/ice cloud delineation is useful for aircraft routing. The 1.6 μm band has a relatively large difference between the imaginary refraction components between water and ice (Baum et al., 2000).

The 2.26 μm band is used for determining cloud particle size; particle growth is an indication of cloud growth and intensity of that growth (Kaufman et al 1997). Other uses of the 2.26 μm band include aerosol particle size (by characterizing the aerosol-free background over land), cloud screening, hot spot detection, snow detection and total moisture determinations. The MODIS cloud mask algorithm employs a similar band (Ackerman et al., 1998).

3.3 Infrared bands

The shortwave IR window (3.9 μm) band has many uses on the current GOES imagers including fog (Ellrod et al. 1998) and low-cloud discrimination at night, fire identification (Prins et al., 1998), volcanic eruption and ash detection, and daytime reflectivity for snow and ice. Due to the increased sensitivity to temperature, this ABI band can also be used to study urban heat island affects.

The 6.2 and 7 μm band applications include upper-level tropospheric water vapor tracking, jet stream identification, hurricane track forecasting, mid-latitude storm forecasting, severe weather analysis, and upper level moisture estimation. These bands may also be used for a number of broadcast applications. Using both MODIS and current GOES data, the improved spatial resolution of the ABI is demonstrated in Figure 7. The "herring bone pattern" evident in the higher spatial resolution data is revealing moisture structures. This scene is completely clear (with the exception of some low fog).

The 7.34 μm band reveals flow information of the mid and lower levels. It can also identify jet streaks. Along with the other water vapor bands, some vertical moisture information can be assessed. This band also helps identifying and tracking volcanic plumes via absorption due to SO_2.

The 8.5 μm band can be combined with the 11.2 and 12.3 μm bands to derive top-cloud phase (Strabala et al. 1994). This determination of the microphysical properties of clouds includes a more accurate and consistent delineation of ice clouds from water clouds during the day or night. In addition, the 8.5 μm band, in conjunction with the 11.2 and 12.3 μm band, will enable detection of volcanic dust clouds containing sulfuric acid aerosols (Realmuto et al. 1997; Ackerman and Strabala 1994). Other uses of the 8.5 μm band include thin cirrus detection in conjunction with the 11.2 μm band (to improve other products by reducing cloud contamination), better atmospheric correction in relatively dry atmospheres (to improve SST), and estimation of surface properties in conjunction with the 10.35 μm band.

The addition of a thermal ozone channel (9.6 μm) on the GOES-R Imager will provide information both day and night about the dynamics of the atmosphere near the tropopause on both high spatial and temporal resolutions (Li et al. 2001, Schmidt et al. 2004). Significant wind shear, turbulence, and tropopause folding occur in the middle latitudes, particularly during the baroclinic storms in the spring and fall. A high temporal and spatial ozone product derived from the 9.6 μm may give some indications to clear-air turbulence.

The 10.35 μm atmospheric window band is less sensitive to low-level moisture and hence helps estimates of atmospheric corrections, cloud particle size and surface properties. Chung et al. (2000) showed how the 10 - 11 μm region is important for determining particle sizes of ice-clouds.

The longwave infrared window (11.2 μm) band provides day/night cloud analyses for general forecasting and broadcasting applications, precipitation estimates (Vicente et al., 1998), severe weather analyses, cloud drift winds (Velden et al. 1998a), hurricane strength (Velden et al. 1998b) and track analyses, cloud top heights, volcanic ash detection (Prata 1989), fog detection in multi-band products (Lee et al. 1997), winter storms, and cloud phase/particle size estimates in multi-band products. A convective storm observed by both the current GOES imager and MODIS demonstrates the improved spatial resolution of the ABI data (Figure 8). The "warm wake" or "enhanced v" is much more evident in the higher resolution data. Also, concentric circles, indicating cloud-level gravity waves, are seen in the higher spatial resolution ABI data, but not the poorer spatial resolution GOES data. It is possible that these waves could be used as an indicator of turbulence. The MODIS data were averaged to 2km to represent the spatial resolutions of the ABI.

The 12.3 μm band offers nearly continuous cloud monitoring for numerous applications including low-level moisture determinations, volcanic ash identification detection (Davies and Rose 1998), Sea Surface Temperature (SST) measurements (Wu et al. 1999), and cloud particle size (in multi-band products). It has been shown that mid-level dust amounts (from the Saharan Air Layer) maybe useful in determining hurricane intensification in the Atlantic basin (Dunion and Velden, 2004).

The 13.3 μm band is used for cloud top height assignments for cloud-drift winds, high cloud products supplementing ASOS (Automated Surface Observing System) observations (Schreiner et al. 1993; Wylie and Menzel 1999), tropopause delineation, and estimation of cloud opacity. These cloud products will be further improved by combining the data with high-spectral resolution sounder data (Li et al, 2004a, Li et al, 2004b). These products will be useful for aviation weather forecasters, numerical weather prediction (for analysis and/or validations), and possibly the VAAC (Volcanic Ash Advisory Center) for determining heights of ash clouds. Products using the 13.3 μm are being demonstrated with the GOES-12+ imagers (Schreiner and Schmit, 2001; Hillger et al 2003).

The next generation METEOSAT (launched in 2002 and now referred to as MET-8) has 12 bands, including a number of the infrared bands selected for ABI (Schmetz et al., 1998; Schmetz et al., 2002, Woick et al., 1997). These data, along with other ABI simulated data from MODIS, AIRS or forward model calculations, will be used to prepare for ABI.

Select imager products and the primary and secondary bands used to compute those products are listed in Table 3. HES refers to a product from the combined imager/sounder system. Table 4 is a comparison between the current and ABI imagers. The specified instrument noise for most bands are 0.1K (although the 13.3 μm band is 0.3K), all referenced at 300K. The ABI is also expected to have on-orbit visible calibration; while the current GOES instruments do not.

A sample “16 band” ABI multiple panel image from April 11, 2004 at approximately 13 UTC is shown in Figure 9. This image over France is built from measurements from three separate satellite instruments (MODIS, MET-8 and AIRS). Bands from each sensor are needed, given the various bands and spectral coverage. The spectral simulation is more representative for those bands derived from the high-spectral resolution AIRS data due to convolution step. The spatial information is more representative for those bands derived from higher spatial resolution MODIS data. The 1.38 μm band is dark because it is centered within an absorption band. Note that the snow covered Alps are bright (reflective) in the first three visible bands, while it is darker (absorbing) in both the 1.6 and 2.2 μm bands. The "2.2 μm " band is actually 2.1 μm because it is from MODIS. The ABI will allow similar multi-spectral full disk observation every 5 or 15 minutes.

4. BAND SELECTION

Each ABI band has been chosen to better met user requirements by building upon the experience with space-borne instruments and/or experience with data from various research aircraft. The channel selection for ABI is a balance of heritage with existing GOES imager bands (between the GOES-8/11 and GOES-12/P series), the current GOES Sounder bands, complementarity with bands on other operational and research satellites in both geostationary and polar-orbits (e.g, MODIS and Meteosat Second Generation), and possible synergy with information derived from advanced high-spectral resolution sounders. While any given ABI band have been based on several instruments, the primary heritage instrument for each band is summarized in Table 5.

The 0.47 μm band is based on a MODIS band. A similar band has flown on a number of other satellites, including SeaWIFS (Sea-viewing Wide Field of view Sensor) and is planned for the VIIRS (Visible/Infrared Imager and Radiometer Suite) instrument. The ABI will not be the first geostationary sensor to carry this "blue" band because ATS-3, launched in 1967, provided the first color image of the entire Earth via a Multicolor Spin Scan Cloud Camera. The 0.64 μm band is based on the current GOES Imager and Sounder bands, although a visible band in this spectral range has flown on geostationary imagers since the 1960s. For example, the Applications Technology Satellite (ATS) series. first launched on December 7, 1966, carried an instrument capable of providing images of the full disk.

The 0.86 μm band is based on a similar polar-orbiting AVHRR (Advanced Very High Resolution Radiometer) band, but it has been spectrally narrowed to minimize influence of a water vapor absorption feature near 0.80 μm. This mitigates the effect that atmospheric changes would have on surface products (M. Griffin, personal communication, Sieglaff et al, 2003). The 1.38 μm band is based on MODIS and MAS (MODIS Airborne Simulator) aircraft data. The MAS has a similar-type band at 1.88 μm. The 1.6 μm band is based on AVHRR experience, but has been narrowed (more like the spectral width of the corresponding MODIS band) to give a less ambiguous phase determination. The 2.26 μm band is similar to the 2.1 μm band on MODIS, but has been shifted spectrally for a better particle size determination (King et al 2003).

The 3.9 μm band is based on the current GOES Imager band 2, although similar bands are on the AVHRR and other instruments such as the VAS (VISSR (Visible and Infrared Spin-Scan Radiometer) Atmospheric Sounder). The 6.19 μm band is based on the current GOES Imager and Meteosat-8. The 6.95 μm is similar to bands on the current GOES Sounder and Meteosat-8. The 7.34 μm band is based on the current GOES Sounder and a similar MODIS band, although this band has been shifted to better detect upper-level SO_2. The 8.5 μm band is similar to a MODIS band. Meteosat-8 carries a similar channel (8.5 to 8.9 μm). The spectral width of the ABI was based on the MAS. The 9.6 μm band was spectrally widened with respect to traditional ozone- sensitive infrared bands to minimize the sensitivity to the spectral response function cutoff being in a spectral region of rapidly changing brightness temperatures. The 10.35 μm band is based on experience with the MAS. The longwave infrared window (11.2 μm) band is similar to many bands on past and existing instruments. The 12.3 μm band, or part of the "split window", is similar to bands on both the GOES-8/11 Imagers and the current Sounder. The 13.3 μm band is similar to a band both on the current GOES-12/N/O/P Imager and Sounder.

5. SUMMARY

The ABI represents an exciting expansion in geostationary remote sensing capabilities. The ABI addresses the needs of the National Weather Service (and others) by increasing spatial resolution (to better monitor small-scale features), by scanning faster (to improve temporal sampling and to scan additional regions) and by adding spectral bands (to enable new and improved products for a wide range of phenomena). Every product that is being produced from the current GOES Imager will be improved with data from the ABI. Plus, several new products will be possible that exploit the

improved spectral, temporal and spatial resolutions. Learning from existing data sets, both from operational and research satellites are one way to prepare for the use of the ABI data.

Where appropriate, products will be produced in concert with the GOES-R high-spectral resolution sounder. It has been shown that several products can be improved when using high spatial resolution imager data with co-located high-spectral resolution measurements, MODIS/AIRS investigations are revealing possible ABI/HES synergy. Also, the GOES system complements the polar systems and the entire Global Observing System (GOS).

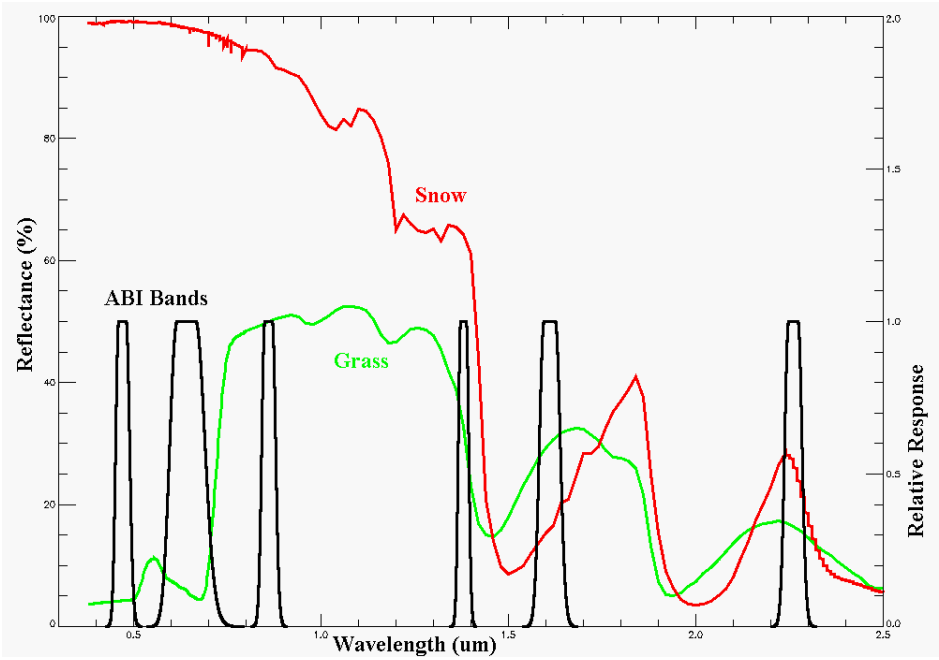

Figure 1. The spectral coverage of the six visible/near infrared bands along with two representative high-spectral resolution spectral plots. The current GOES imager only has one visible band centered near 0.65 μm.

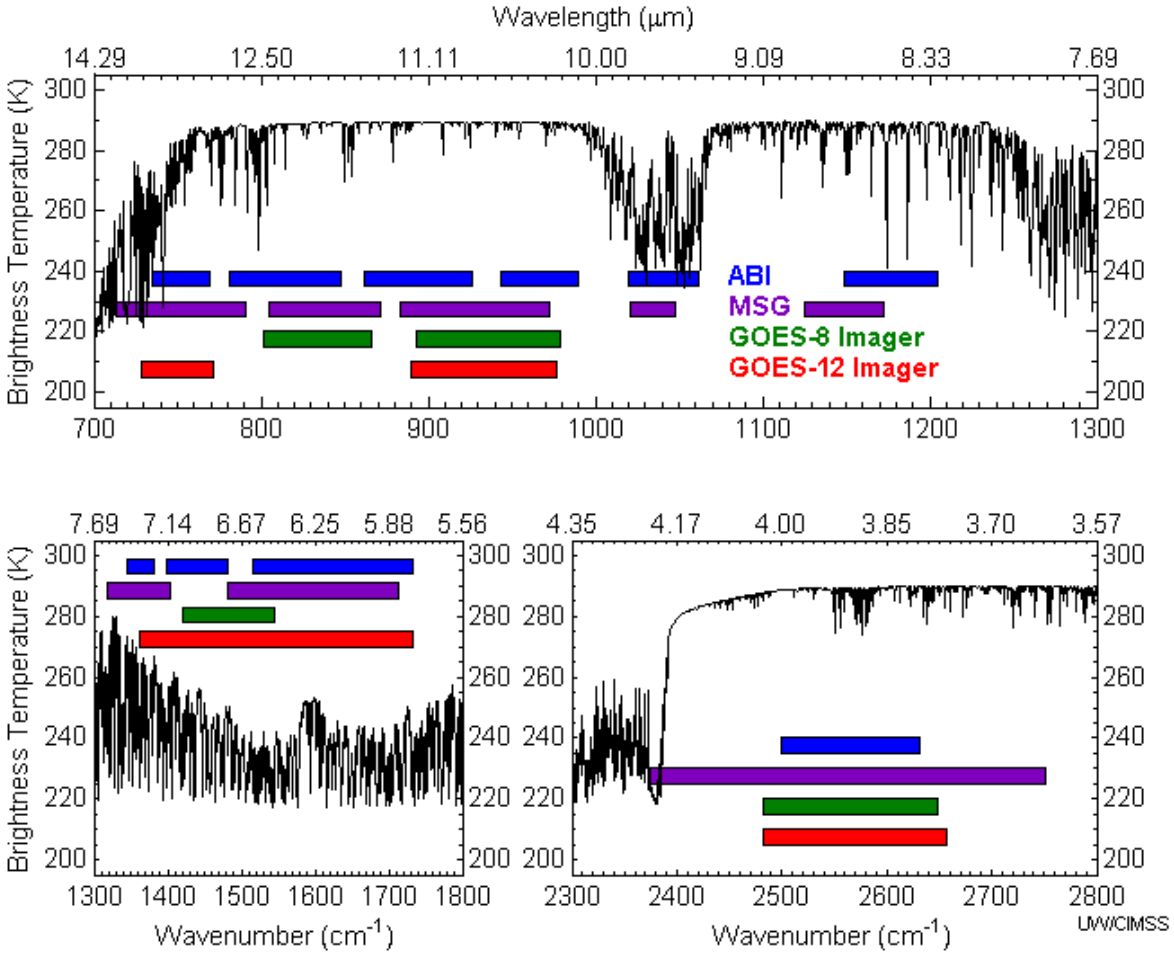

Figure 2. The spectral coverage of the ten ABI bands in the infrared region. These are compared with an earth-emitted calculated spectrum from the standard U.S. atmosphere. The spectral coverage from the GOES-8 and -12 imagers, along with those from the Meteosat Second Generation (MSG) are also shown.

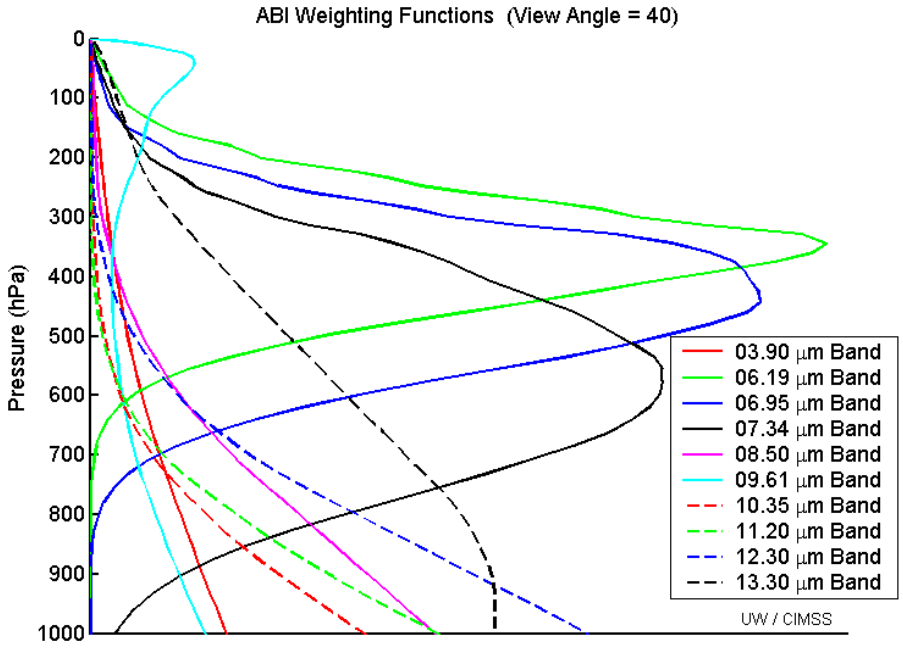

Figure 3. The ABI weighting functions are plotted for the U.S. standard atmosphere at a local zenith angle of 40 degrees.

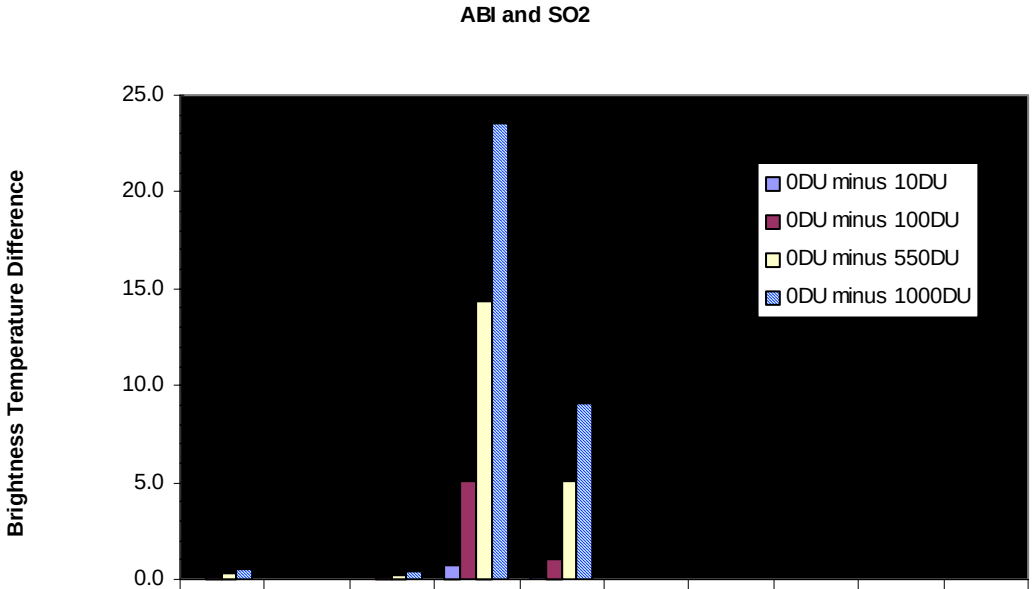

	3.9	6.18	6.95	7.34	8.5	9.61	10.4	11.2	12.3	13.3
0DU minus 10DU	0.012	0.001	0.012	0.685	0.116	0.001	0.000	0.000	0.000	0.000
0DU minus 100DU	0.059	0.001	0.087	5.092	1.073	0.002	0.000	0.000	0.000	0.000
0DU minus 550DU	0.278	0.001	0.255	14.329	5.094	0.010	0.000	0.000	0.000	0.000
0DU minus 1000DU	0.496	0.002	0.423	23.566	9.114	0.017	0.000	0.000	0.000	0.000

ABI Band

UW/CIMSS

Figure 4. Forward model calculations of the effect of various amounts of SO_2 on the ABI bands. The ordinate is the difference between calculated atmospheres with no SO_2 and those with SO_2. Note that the ABI should be able to detect medium to large amounts, but not small amounts.

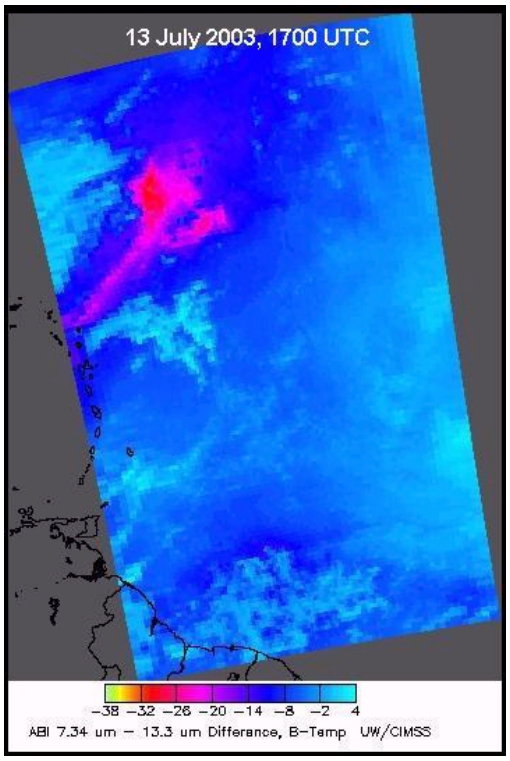

Figure 5. AIRS data (July 13, 2003 at 17 UTC) convolved to simulate the spectral characteristics of two ABI bands. A difference image is shown between the 7.34 and 13.3 μm bands. The image shows the location of a SO_2 plume. Independent SO_2 retrievals (not shown) from both AIRS and TOMS (Total Ozone Mapping Spectrometer) show amounts between 100 and 500 Dobson Units (DU) for this case.

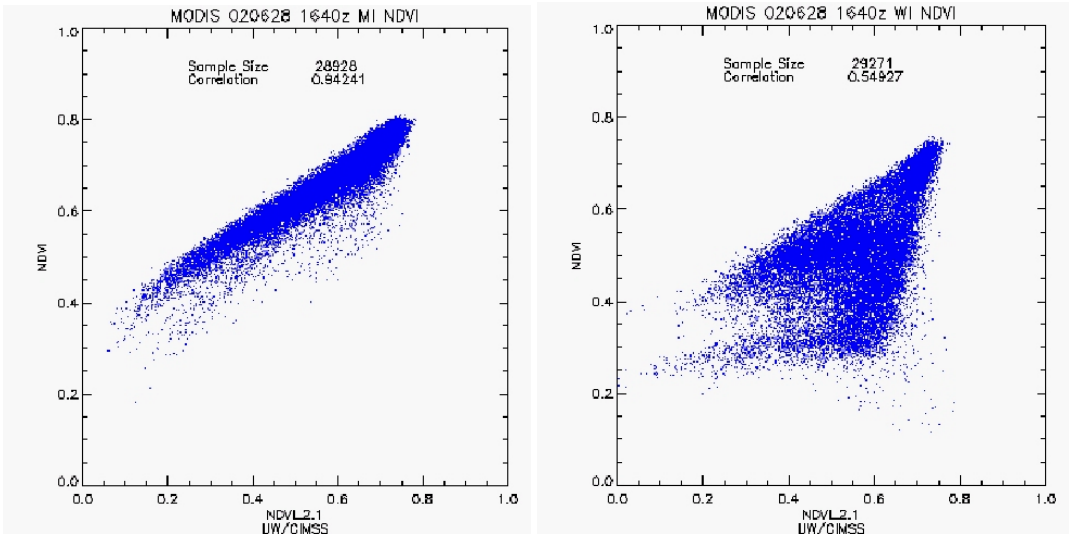

Figure 6. Calculated NDVI using MODIS data from 1640 UTC 28 June 2002. The left panel is the traditional NDVI compared to a NDVI product using the MODIS 2.1 μm for a clear scene, while the right panel is for a smoky scene. Note that the traditional NDVI product seems to be affected by smoke. Of course these smoky regions could be masked out, but that would limit the amount of information of the surface vegetation.

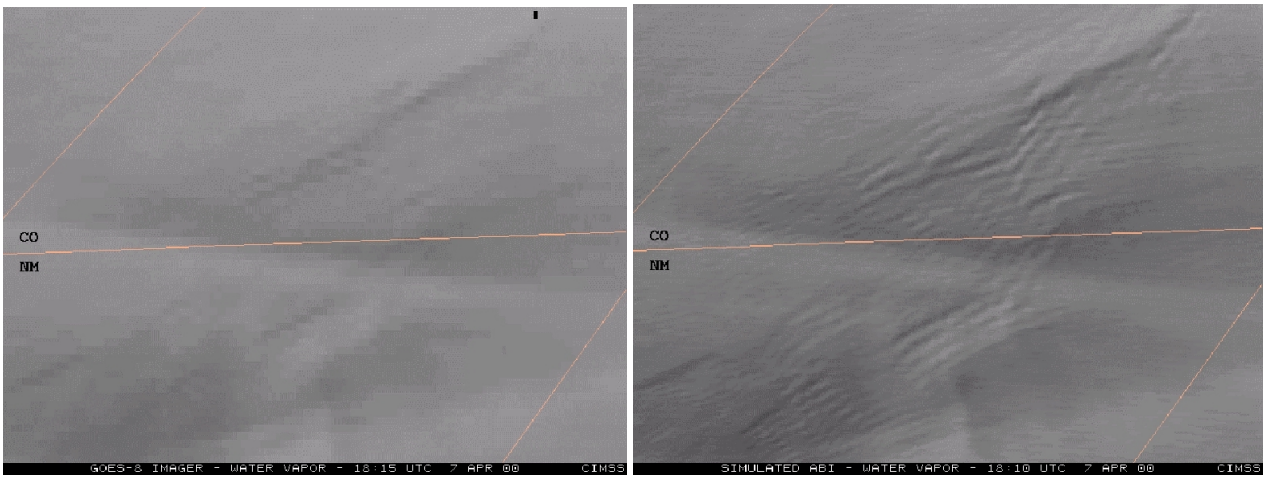

Figure 7. Improved spatial resolution of the water vapor bands of the ABI demonstrated in mountain waves. Note that this is a cloud-free scene, so all the structure is due to mesoscale variability in mid-tropospheric water vapor. Mountain waves over Colorado and New Mexico were induced by strong northwesterly flow associated with a pair of upper-tropospheric jet streaks moving across the elevated terrain of the southern and central Rocky Mountains. The mountain waves appear better defined over Colorado, where there were aircraft reports moderate to severe turbulence.

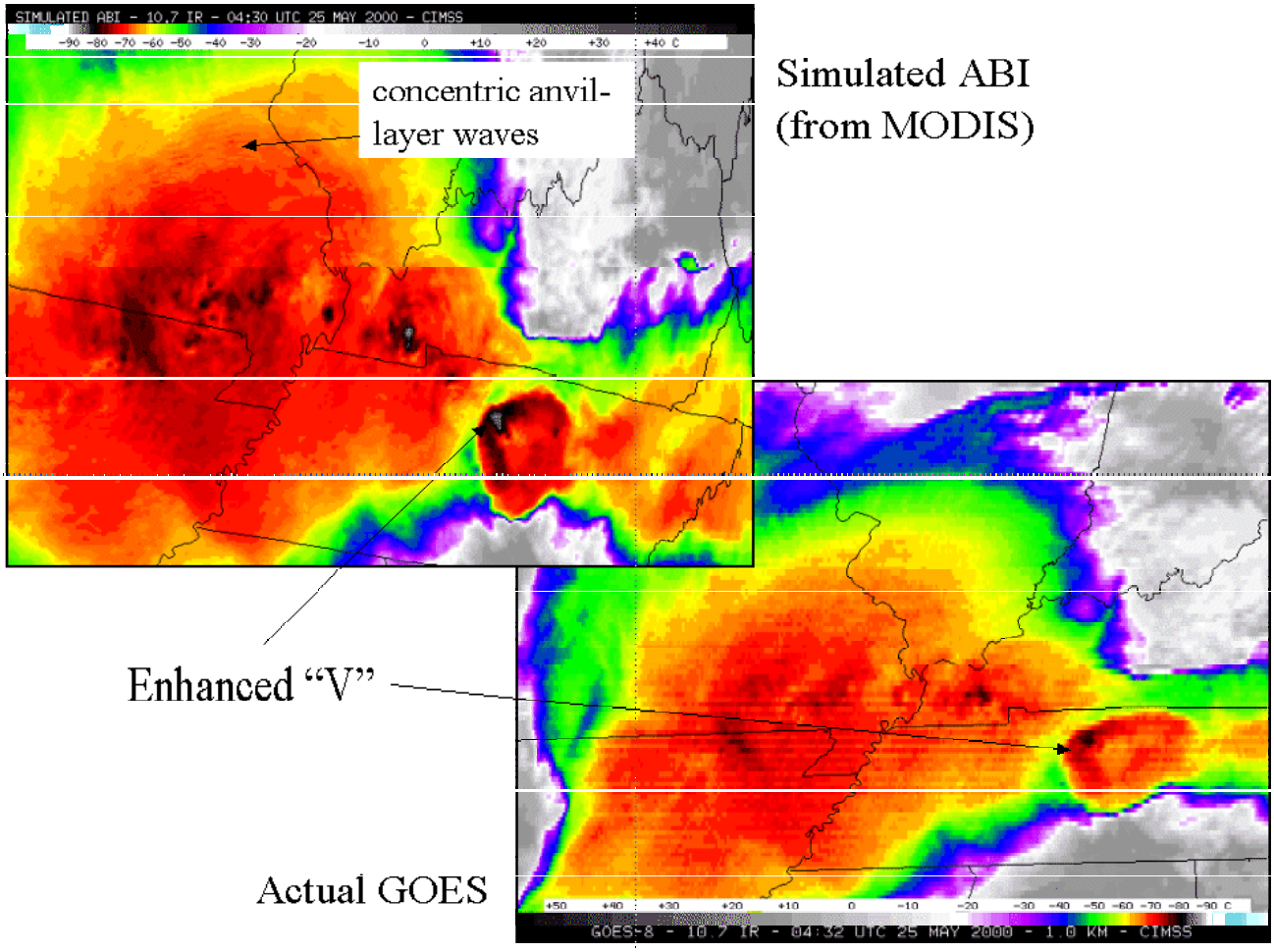

Figure 8. Improved spatial resolution of the infrared window bands of the ABI demonstrated for a convective cloud case. Note the sharper Enhanced "V" signature in the infrared window on May 25, 2000. Also of note is the concentric anvil-layer waves observable in the higher spatial resolution data. These waves are associated with rapidly developing cells.

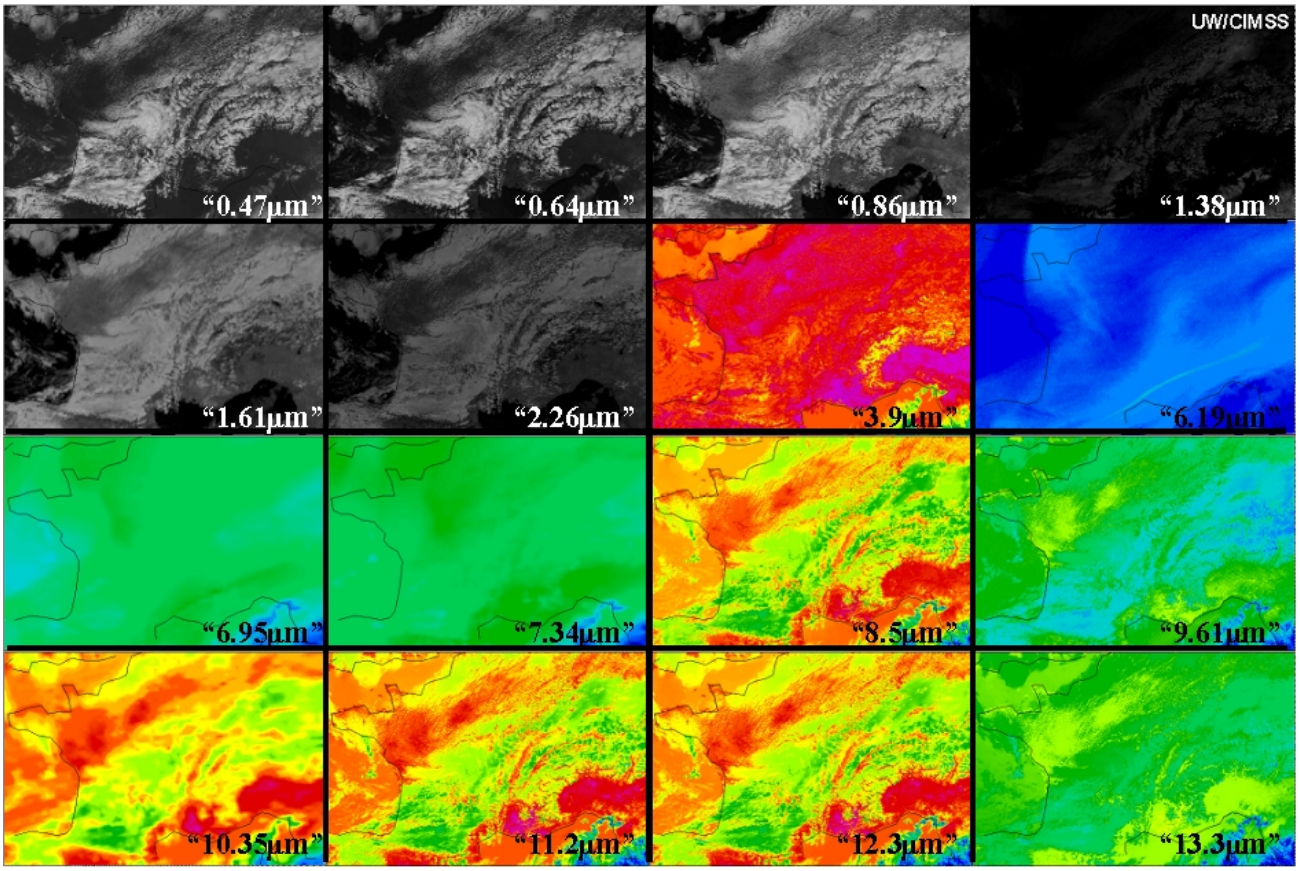

Figure 9. A simulated "16 band" ABI multiple panel image from April 11, 2004 at approximately 13 UTC. This image over France is built from measurements from three separate satellite instruments (MODIS, MET-8 and AIRS).

Table 1. Summary of the bands on the current GOES Imagers from Hillger et al. (2003). The minimum and maximum wavelength range represent the half-max 50% points. IGFOV is the Instantaneous Geometric Field Of View.

Current GOES Imager Band	**Approximate Wavelength Range (µm)**	**Central Wavelength (µm)**	**Nominal sub-satellite IGFOV (km)**	**Sample Use**
1	0.53 to 0.75	0.65	1	Cloud cover and surface features during the day
2	3.8 to 4.0	3.9	4	Low cloud/fog and fire detection
3	6.5 to 7.0 5.8 to 7.3	6.75 **(GOES-8/11)** 6.48 **(GOES-12+)**	8 4	Upper-level water vapor
4	10.2 to 11.2	10.7	4	Surface or cloud top temperature
5	11.5 to 12.5	12.0 **(GOES-8/11)**	4	Surface or cloud top temperature and low-level water vapor
6	12.9 to 13.7	13.3 **(GOES-12/N)** 13.3 **(GOES-O/P)**	8 4	CO_2 band: Cloud detection

Table 2. Summary of the bands on the future GOES Imagers (ABI). The minimum and maximum wavelength range represent the half-max 50% points.

Future GOES Imager (ABI) Band	Wavelength Range (µm)	Central Wavelength (µm)	Nominal sub-satellite IGFOV (km)	Sample Use
1	0.45-0.49	**0.47**	**1**	Daytime aerosol-over-land, coastal water mapping
2	0.59-0.69	**0.64**	**0.5**	Daytime clouds fog, insolation, winds
3	0.84-0.88	**0.86**	**1**	Daytime vegetation/burn scar & aerosol-over-water, winds
4	1.365-1.395	**1.38**	**2**	Daytime cirrus cloud
5	1.58-1.64	**1.61**	**1**	Daytime cloud-top phase, snow
6	2.235 - 2.285	**2.26**	**2**	Daytime land/cloud properties, particle size, vegetation, snow
7	3.80-4.00	**3.90**	**2**	Surface & cloud, fog at night, fire, winds
8	5.77-6.6	**6.19**	**2**	High-level atmospheric water vapor, winds, rainfall
9	6.75-7.15	**6.95**	**2**	Mid-level atmospheric water vapor, winds, rainfall
10	7.24-7.44	**7.34**	**2**	Lower-level water vapor, winds & SO2
11	8.3-8.7	**8.5**	**2**	Total water for stability, cloud phase, dust, SO2, rainfall
12	9.42-9.8	**9.61**	**2**	Total ozone, turbulence, and winds
13	10.1-10.6	**10.35**	**2**	Surface & cloud
14	10.8-11.6	**11.2**	**2**	Imagery, SST, clouds, rainfall
15	11.8-12.8	**12.3**	**2**	Total water, ash, and SST
16	13.0-13.6	**13.3**	**2**	Air temperature, cloud heights and amounts

Table 3. Select imager products and needed spectral coverage from the ABI. The column labeled HES reflects product that can be improved with high spectral infrared data from the HES.

Sample Product list	**Primary ABI Band(s) (μm)**	**Secondary ABI Band(s) (μm)**	**HES**
aerosols/dust/smoke	0.47, 2.2, 8.5, 12.3	0.64, 0.86, 1.6, 10.3, 11.2	Yes.
clear sky masks (Imager)	0.64,1.38, 8.5,11.2,12.3	0.47,0.86, 1.6, 8.5,13.3	
cloud imagery	0.64, 1.38, 3.9, 11.2, 13.3	0.86, 8.5, 10.35	Yes.
cloud-top microphysics	0.64, 1.6, 3.9, 10.35, 11.2	0.86, 2.2, 8.5	Yes.
cloud-top phase	1.6, 8.5, 11.2, 13.3	0.6, 1.38, 2.2	Yes.
cloud-top pressure/temperature	8.5, 11.2, 13.3	3.9, 6.15, 7, 10.3,13.3	Yes.
fires/hot spots	3.9, 11.2	0.64, 2.2, 12.3, 13.3	
fire burn scars	0.86	0.64, 10.3	
hurricane intensity	11.2	0.64, 3.9, 6.15, 8.5, 13.3	Yes.
insolation	0.47, 0.64	0.86, 1.6	
land skin temperature	3.9, 11.2, 12.3	7.3, 8.5, 10.3	Yes.
low cloud and fog	3.9, 11.2	0.64, 1.61, 10.3, 12.3	Yes.
rainfall rate/QPE	8.5, 11.2, 12.3, 13.3	0.64, 6.15, 7.3, 10.3	Yes.
derived motion	0.64, 3.9, 6.19, 7, 7.3,11.2	0.86, 1.38, 9.7, 10.3, 12.3, 13.3	Yes.
sea ice products	0.64, 1.6	2.2, 3.9, 11.2, 12.3	
sea surface temperature	3.9, 11.2, 12.3	8.5, 10.35	Yes.
snow detection (cover)	1.61	0.64, 0.86, 2.2, 3.9, 11.2	
SO_2 concentration (upper-level)	8.5, 7.34	9.6, 11.2, 13.3	Yes.
surface properties	8.5, 10.35	11.2	Yes.
suspended sediment	0.64, 0.86	0.47	
total ozone	9.6	11.2, 13.3	Yes.
turbulence	6.15, 7, 9.6	7.3, 11.2, 13.3	
vegetation index	0.86	0.64, 2.2	
volcanic ash product	0.64, 3.9, 8.5, 12.3	7.3, 11.2, 13.3	Yes.

Table 4. Comparison of the current and future geostationary imagers. It should be noted that the instrument noise values for ABI are specifications, while those from the GOES Imager are on-orbit measurements.

Parameter	**Current GOES Imager**	**Future GOES Imager**	**Comments**
Visible bands	1	3	Cloud cover, plant health and surface features during the day
Near IR bands	0	3	Cirrus clouds, Low cloud/fog and fire detection
Infrared bands	4	10	Upper-level water vapor, clouds, SO_2, SST, etc
Coverage Rate	25 minutes for full disk	Approximately 5 minutes for full disk	Approximately five times faster
Noise (at 300K) in the IR window	0.15K	0.10K	No correction has been made for the larger FOV of the current GOES imager compared to that of the ABI
Spatial resolutions of the infrared bands	4-8 km	2 km	At the sub-satellite point
Low-light capabilities	No	Yes	

Table 5. Summary of the ABI bands and sample heritage instruments.

Future GOES Imager (ABI) Band	Central Wavelength (μm)	Primary Heritage Instrument
1	**0.47**	MODIS
2	**0.64**	current GOES Imager
3	**0.86**	spectrally modified AVHRR
4	**1.38**	MODIS and MAS
5	**1.61**	Spectrally modified AVHRR
6	**2.26**	Similar to MODIS
7	**3.90**	current GOES Imager
8	**6.19**	current GOES Imager
9	**6.95**	current GOES Sounder
10	**7.34**	spectrally modified current GOES Sounder
11	**8.5**	MAS
12	**9.61**	spectrally modified current Sounder
13	**10.35**	MAS
14	**11.2**	current GOES Sounder
15	**12.3**	current GOES Sounder
16	**13.3**	current GOES Sounder/GOES-12+ Imager

ACKNOWLEDGMENTS

The authors would like to thank a host of scientists at CIMSS, NOAA/NESDIS, NASA and other agencies that contributed to ABI band selection. This includes Steve Ackerman, Bryan Baum, Dennis Chesters, Monica Coakley, Gary Ellrod, James P. Nelson III, Art Neuendorffer, Dan Flanagan, Elaine Prins, Fred Prata, Michael K. Griffin, Andrew Heidinger, Don Hillger, Allen Huang, Bob Kuligowski, Chris Moeller, Fred Mosher, Robert Rabin, Jo Schmetz, Chris Schmidt, Anthony Schreiner, Micheal Weinreb and Harold Woolf. University of Wisconsin—Madison undergraduate students Justin Sieglaff and Kris Karnauskas are also thanked for their work with the AVIRIS, MODIS and AIRS data. The simulated ABI Spectral Response Files are available upon request. The cost benefit study is on-line at: *http://www.osd.noaa.gov/goes_R/docs/GOES-R_CBA_Final_Jan_9_2003.pdf*. The spectra data in Figure 1 are from the ASTER library at: http://speclib.jpl.nasa.gov/. This work was supported under grant number: NA07EC0676. The views, opinions, and findings contained in this paper are those of the authors and should not be construed as an official National Oceanic and Atmospheric Administration or U.S. Government position, policy, or decision.

REFERENCES

Ackerman, S. A., and H. Chung, 1992: Radiative effects of airborne dust on regional energy budgets at the top of the atmosphere. *J. Atmos. Sci.*, **31**, 223–236.

Ackerman, S. A., 1996: Global satellite observations of negative brightness temperature differences between 11 and 6.7 µm. *J. Atmos. Sci.*, **53**, 2803–2812.

Ackerman, S. and K. I. Strabala, 1994: Satellite remote sensing of H_2SO_4 aerosol using the 8 to 12 µm window region: Application to Mount Pinatubo. *J. Geo. Res.*, **99**, 18,639-18,649.

Ackerman, S. A., K. I. Strabala, W. P. Menzel, R. A. Frey, C. C. Moeller, and L. E. Gumley, 1998: Discriminating clear sky from clouds with MODIS. *J. Geophys. Res*., **103**, 32141-32157.

Aquirre-Gomez, R., 2000: Detection of total suspended sediments in the North Sea using AVHRR and ship data. *Int. J. Remote Sensing*, **21**, 1583-1596.

Aumann, H. H., M. T. Chahine, C. Gautier, M. D. Goldberg, E. Kalnay, L. M. McMillin, H. Revercomb, P. W. Rosenkranz, W. L. Smith, D. H. Staelin, L. L. Strow, and J. Susskind, J., 2003: AIRS/AMSU/HSB on the Aqua mission: design, science objectives, data products, and processing systems. *IEEE Trans on Geosci. and Remote Sensing*, NO. 2, 41, 253- 264.

Ba, M., and A. Gruber, 2001: GOES Multispectral Rainfall Algorithm (GMSRA). *J. Appl. Meteor*., Vol. 40, No. 8, 1500–1514.

Barton, I. J., A. J. Prata, I. G. Watterson, and S. A. Young, 1992: Identification of the Mount Hudson volcanic cloud over SE Australia. *Geophys. Res. Lett.*, **19**, 1211-1214.

Bayler, G. M., R. M. Aune, and W. H. Raymond, 2001: NWP cloud initialization using GOES sounder data and improved modeling of non-precipitating clouds. *Mon. Wea. Rev*., **128**, 3911-3920.

Baum, B. A., P. F. Soulen, K. I. Strabala, M. D. King, S. A. Ackerman,W. P. Menzel, and P. Yang, 2000: Remote sensing of cloud properties using MODIS Airborne Simulator imagery during SUCCESS. II. Cloud thermodynamic phase. J. Geophys. Res., 105, 11,781-11,792.

Bosart, L. F., C. S. Velden, W. E. Bracken, J. Molinari, and P. G. Black, 2000: Environmental influences on the rapid intensification of Hurricane Opal (1995) over the Gulf of Mexico. *Mon. Wea. Rev.*, **128**, 322–352.

Casadevall, T.J., 1992: Volcanic hazards and aviation safety: Lessons of the past decade, *FAA Aviation Safety Journal*, 2 (3), 1-11.

Chung S., S. Ackerman, and P. F. van Delst, 2000: Model calculations and interferometer measurements of ice-cloud characteristics. *J. Appl. Met*., **39**, 634-644.

Davies, M. A., and W. I. Rose, 1998: Evaluating GOES imagery for volcanic cloud observations at the Soufriere Hills volcano, Montserrat. *EOS Trans A G U, 79:505-507*.

Diak, G. R., M. C. Anderson, W. L. Bland, J. M. Norman, J. M. Mecikalski, and R. A. Aune, 1998: Agricultural management decision aids driven by real time satellite data. *Bull. Amer. Meteor. Soc*., **79**, 1345-1355.

Dostalek, J. F., J. F. Weaver, J. F. W. Purdom, K. Y. Winston, 1997: PICTURE OF THE QUARTER: Nighttime Detection of Low-Level Thunderstorm Outflow Using a GOES Multispectral Image Product. Weather and Forecasting: Vol. 12, No. 4, 947–950.

Dunion, J.P., and C.S. Velden, 2004: The impact of the Saharan Air Layer on Atlantic tropical cyclone activity. *Bull. Amer. Meteor. Soc*., Vol. 85, No. 3, pp. 353–365.

Ellrod, G. P., 1996: The use of GOES-8 multispectral imagery for the detection of aircraft icing regions. Preprint Volume, *8th Conf. on Satellite Meteorology and Oceanography*, Atlanta, Georgia, Amer. Meteor. Soc., Boston, 168-171.

Ellrod, G. P., 2001: Loss of the 12.0 um "split window" band on GOES-M: Impacts on volcanic ash detection. *11th Conference on Satellite Meteorology and Oceanography*, 15—18 October, Madison, WI.

Ellrod, G. P., R. V. Achutuni, J. M. Daniels, E. M. Prins, and J. P. Nelson III, 1998: An assessment of GOES-8 Imager data quality, *Bull. Amer. Meteor. Soc.*, **79**, 2509-2526.

Frey, R. A., B. A. Baum, W. P. Menzel, S. A. Ackerman, C. C. Moeller, and J. D. Spinhime, 1999: A comparison of cloud top heights computed from airborne LIDAR and MAS radiance data using CO_2-slicing, *J. Geophys. Res.*, **104**, 24,547-24,555.

Garand, Louis. 2003: Toward an Integrated Land–Ocean Surface Skin Temperature Analysis from the Variational Assimilation of Infrared Radiances. *J Applied Meteorology*: Vol. 42, No. 5, pp. 570–583.

Gao, B.-C., P. Yang, W. Han, R. R. Li, and W. J. Wiscombe, 2002: An algorithm using visible and 1.375 μm channels to retrieve cirrus cloud reflectances from aircraft and satellite data. *IEEE Transactions on Geoscience and Remote Sensing*, 40, 1659 – 1688.

Goerss, J. S., C. S. Velden, and J. D. Hawkins, 1998: The impact of multispectral GOES-8 wind information on Atlantic Tropical Cyclone track forecasts in 1995. Part II: NOGAPS Forecasts. *Mon. Wea. Rev*, **126**, 1219–1227.

Gurka J. J., and G. J. Dittburner, 2001: The next generation GOES instruments: status and potential impact. Preprint Volume. 5th Symposium on Integrated Observing Systems. 14-18 January, Albuquerque, NM., Amer. Meteor. Soc., Boston.

Gu, Y., W. I. Rose, G. J. S. Bluth, 2003: Retrieval of mass and sizes of particles in sandstorms using two MODIS IR bands: A case study of April 7, 2001 sandstorm in China. GEOPHYSICAL RESEARCH LETTERS, VOL. 30, NO. 15, 1805, doi:10.1029/2003GL017405.

Hannon, S, L. L. Strow, and W. W. McMillan, 1996: In Proceeding of SPIE conference 2830, Optical Spectroscopic Techniques and Instrumentation for Atmospheric and Space Research II.

Hayden, C. M., G. S. Wade, and T. J. Schmit, 1996: Derived product imagery from GOES-8. *J. Appl. Meteor*., **35**, 153-162.

Hillger, D. W., 1996: Meteorological features from principal component image transformation of GOES imagery, Proceedings, *GOES-8 and Beyond*, Intl. Soc. Optical Engineering, Denver, Colorado, 111-121.

Hillger, D. W., and J. Clark, 2002: Principal Component Image Analysis of MODIS for Volcanic Ash, Part-2: Simulation of Current GOES and GOES-M Imagers, *J. Appl. Meteor*., Vol. 41, No. 10, 1003–1010.

Hillger, D. W., T. J. Schmit, and J. M. Daniels, 2003: Imager and sounder radiance and product validations for the GOES-12 science test, NOAA Technical Report 115, U.S. Department of Commerce, Washington, DC.

Hutchison, K. D., 1999: Application of AVHRR/3 imagery for improved detection of thin cirrus clouds and specification of cloud-top phase. *J. Atmos. Oceanic Tech*., **16**, 1885-1899.

Karnieli, A., Y. J. Kaufman, L.A. Remer, A. Wald, 2001: AFRI - aerosol free vegetation index, Remote Sensing of Environment, **77**, 10-21, 2001.

Kaufman, Y.J., A.E. Wald, L.A. Remer, B.- C. Gao, R.- R. Li and L. Flynn 1997: The MODIS 2.1 um Channel - Correlation with visible reflectance for use in remote sensing of aerosol., IEEE Trans. Geo, 35, 1286-1298.
King, M.D., W. P. Menzel, Y. J. Kaufman, D. Tanre, B. Gao, S. Platnick, S. A. Ackerman, L. A. Remer, R. Pincus, and P. A. Hubanks, 2003: Cloud and aerosol properties, precipitable water, and profiles of temperature and water vapor from MODIS. *IEEE Transactions on Geoscience and Remote Sensing*, 41, No. 2, 442- 458.

Kim, D., and S. G. Benjamin, 2000: Assimilation of cloud-top pressure derived from GOES sounder data into MAPS/RUC. Preprints, *10th Conf. on Satellite Meteorology and Oceanography*, Long Beach, CA, Amer. Meteor. Soc., 110-113.

Kittaka C., Szykman J., Pierce B., Szykman J., Al-Saadi, J., Neil D., Chu A., Prins E., and Holdzkom J, 2004: Utilizing MODIS satellite observations to monitor and analyze MODIS satellite observations to monitor and analyze fine particulate matter (PM fine particulate matter (PM2.5 2.5) transport event. Paper) transport event. Paper no. 1.3 presented at the *84thAnnual AMS Meeting in Seattle, WA, January 1 -15*.

Kogan, F. N., 1990, Remote sensing of weather impacts on vegetation in non-homogeneous areas. *International Journal of Remote Sensing*, 11, 1405–1419.

Lee, T. F., F. J. Turk, K. Richardson, 1997: Stratus and Fog Products Using GOES-8–9 3.9-um Data. *Wea. Forecasting*, Vol. 12, No. 3, 664–677.

Legeckis, R., C. W. Brown, and P. S. Chang, 2002: Geostationary satellites reveal motions of ocean surface fronts. J. Marine Systems, 37, 3–15.

Li, J., C. C. Schmidt, J. P. Nelson III, T. J. Schmit, and W. P. Menzel, 2001: Estimation of total atmospheric ozone from GOES sounder radiances with high temporal resolution. *J. Atmos. Oceanic Technol.*, **18**, 157-168.

Li, J., T. J. Schmit, and W. P. Menzel, 2002, Advanced Baseline Sounder (ABS) for future Geostationary Operational Environmental Satellites (GOES-R and beyond)", Proceeding of SPIE, *Applications with Weather Satellites*, Hangzhou, China.

Li, J., W. P. Menzel, Z. Yang, R. A. Frey, S. A. Ackerman, 2003: High-spectral resolution surface and cloud type classification from MODIS multi-spectral band measurements, *J. Appl. Meteor.*, Vol. 42, No. 2, 204–226.

Li, J., W. P. Menzel, F. Sun, T. J. Schmit, and J. Gurka, 2004a: AIRS sub-pixel cloud characterization using MODIS cloud products. Submitted to *J. Appl. Meteor.*

Li, J., W. P. Menzel, W. Zhang, F. Sun, T. J. Schmit, J. Gurka, and E. Weisz, 2004b: Synergistic use of MODIS and AIRS in a variational retrieval of cloud parameters. Submitted to *J. Appl. Meteor*.

Menzel, W. P., and J. F. W. Purdom, 1994: Introducing GOES-I: The first of a new generation of geostationary operational environmental satellites, *Bull. Amer. Meteor. Soc.*, **75**, 757-781.

Moeller, C. C., S. A. Ackerman, K. I. Strabala, W. P. Menzel, and W. L. Smith, 1996: Negative 11 micron minus 12 micron brightness temperature differences: a second look, *8th Conference on Satellite Meteorology and Oceanography*, Atlanta, GA, Amer. Meteor. Soc. 313-316.

NOAA NESDIS, *GOES Users Conference Report*, U.S. Dept. of Commerce, Boulder, Colorado, May 22-24, 2001. *http://www.osd.noaa.gov/goes_R/goesrconf.htm*

Moody J. L., A. J. Wimmers, and J. C. Davenport, 1999: Remotely sensed specific humidity: development of a derived product from the GOES Imager channel 3, G*eo. Phys. Let.*, **26**, 59-62.

Mosher, F. R., 2001: A Satellite Diagnostic of Global Convection. *11th Conference on Satellite Meteorology and Oceanography*, 15—18 October, Madison, WI.

Nieman, S. J., J. Schmetz, and W. P. Menzel, 1993: A comparison of several techniques to assign heights to cloud tracers. *J. Appl. Meteor*., **32**, 1559-1568.

Platnick, S.; M. D. King, S. A. Ackerman, W. P. Menzel, B. A. Baum, J. C. Riedi, and R. A. Frey, 2003: The MODIS cloud products: algorithms and examples from Terra. *IEEE Transactions on Geoscience and Remote Sensing*, 41, No.2, 459- 473.

Prata, A. J., 1989: Observations of volcanic ash clouds in the 10-12 μm window using AVHRR/2 data. *Int. J. Remote Sens*., **10**, 751-761.

Prins, E. M., J. M. Feltz, W. P. Menzel, and D. E. Ward, 1998: An overview of GOES-8 diurnal fire and smoke results for SCAR-B and 1995 fire season in South America, *J. Geophysical Res.*, **103**, 31821-31835.

Realmuto, V. J., A. J. Sutton, T. Elias, 1997: Multispectral thermal infrared mapping of sulfur dioxide plumes: A case study from the East Rift Zone of Kilauea Volcano, Hawaii, *J. Geophys. Res*., **102**, 15,057-15,072.

Schmit, T. J., E. M. Prins, A. J. Schreiner, and J. J. Gurka, 2001: Introducing the GOES-M imager. *Nat. Wea. Assoc. Digest*. Volume 25 Nos 3,4.

Schmit T. J., W. F. Feltz, W. P. Menzel, J. Jung, A. P. Noel, J. N. Heil, J. P. Nelson III, G. S. Wade, 2002: Validation and use of GOES sounder moisture information, *Wea. Forecasting*, **17**, 139-154.

Schmidt, C., J. Li and F. Sun, 2004: Simulation of and comparison between GIFTS, ABI, and GOES I-M Sounder Ozone estimates and applications to HES. AMS IIPS conference, Seattle, Washington.

Schreiner, A. J., D. A. Unger, W. P. Menzel, G. P. Ellrod, K. I. Strabala, and J. L. Pellett, 1993: A comparison of ground and satellite observations of cloud cover. *Bull. Amer. Meteor. Soc*., 74, 1851-1861.

Schreiner, A. J., and T. J. Schmit, 2001: Derived cloud products from the GOES-M Imager. *11th Conference on Satellite Meteorology and Oceanography*, 15—18 October, Madison, WI.

Schreiner, A. J., T. J. Schmit, and W. P. Menzel, 2001: Trends and observations of clouds based on GOES sounder data. *J. Geophysical Res. –Atmospheres*, **106**, 20,349-20,363.

Seki, M. P., J. J. Polovina, R. E. Brainard, R. R. Bidgare, C. L. Leonard, and D. G. Foley, 2001: Biological enchancement at cyclonic eddies tracked with GOES thermal imagery in Hawaiian waters. *Geophysical Research Letters*, **28** (8), 1583.

Schmetz, J., H. Woick, S. Tjemkes, and J. Rattenborg, 1998: From Meteosat to Meteosat Second Generation, In Proceedings of the Ninth Conference on Satellite Meteorology and Oceanography, Paris, France, Amer. Meteor. Soc., 335-338.

Schmetz, J., P. Pili, S. Tjemkes, D. Just, J. Kerkmann, S. Rota, A. Ratier, 2002: An Introduction to Meteosat Second Generation (MSG). *Bull. Amer. Meteor. Soc.*, Vol. 83, No. 7, 977–992.

Sieglaff, J. M., and T. J. Schmit, 2003: Vegetation monitoring and thin cirrus detection on the next generation GOES imager. 12th Conference on Satellite Meteorology and Oceanography. Long Beach, CA, 9-13 February.

Soden, B. J., and F. P. Bretherton, 1993: Upper tropospheric relative humidity from the GOES 6.7 μm channel: Method and climatology for July 1987. *J. Geophys. Res.*, **98**, 16669-16688.

Strabala, K. I., S. A. Ackerman, and W. P. Menzel, 1994: Cloud properties inferred from 8-12 μm data. *J. Appl. Meteor*, **33**, 212-229.

Szyndel, M., J.-N. Thepaut, and G. Kelly, 2003: Developments in the assimilation of geostationary radiances at ECMWF. EUMETSAT/ECMWF Fellowship Programme, 1st Year Report, 25 pp

Tarpley, J. D., Schnieder, S. R., and Money, R. L., 1984, Global vegetation indices from NOAA-7 meteorological satellite. J. Climate and Applied Meteorology, 23, 4491–4503.

Vane, G., Airborne Visible/Infrared Imaging Spectrometer (AVIRIS), 1987:. *JPL Publ.*, 87-38, Jet Propulsion Lab, Pasadena, CA.

Velden, C. S., C. M. Hayden, S. J. Nieman, W. P. Menzel, S. Wanzong, and J. S. Goerss, 1997: Upper-tropospheric winds derived from geostationary satellite water vapor observations. *Bull. Amer. Meteor. Soc.*, **78** (2), 173-173.

Velden, C. S., T. L. Olander, and R. M. Zehr, 1998a: Development of an objective scheme to estimate tropical cyclone intensity from digital geostationary satellite infrared imagery. *Wea. Forecasting*, **13** (1), 172–186.

Velden, C. S., T. L. Olander, and S. Wanzong, 1998b: The impact of multispectral GOES-8 wind information on Atlantic tropical cyclone track forecasts in 1995. Part I: dataset methodology, description, and case analysis, *Mon. Wea. Rev.*, **126**(5), 1202–1218.

Vicente, G. A., R. A. Scofield, and W. P. Menzel, 1998: The operational GOES infrared rainfall estimation technique, *Bull. Amer. Meteor. Soc.*, Vol. 79 (9), 1883–1898.

Walker, N., S. Myint, A. Babin, and A. Haag, 2003: Advances in satellite radiometry for the surveillance of surface temperatures, ocean eddies and upwelling processes in the Gulf of Mexico using GOES-8 measurements during summer. Geophysical Research Letters, Vol. 30, no. 16, 1854.

Weldon, R. B, and S. J. Holmes, 1991: Water vapor imagery -- interpretation and applications to weather analysis and forecasting, NOAA Technical Report NESDIS 57.

Woick, H., J. Schmetz, and S. Tjemkes, 1997: An introduction to Meteosat Second Generation imagery and products, *1997 Meteorological Data Users' Conference*, Brussels, Belgium.

Wu, Xiangqian, W. P. Menzel, and Gary S. Wade, 1999: Estimation of sea surface temperatures using GOES-8/9 radiance measurements. *Bull. Amer. Meteor. Soc.*, **80 (**6), 1127-1138.

Wylie, D. P., W. P. Menzel, H. M. Woolf, and K. I. Strabala, 1994: Four years of global cirrus cloud statistics using HIRS. *J. Climate*, **7**, 1972-1986.

Wylie, D. P., and P. H. Wang, 1997: Comparison of cloud frequency data for the High Resolution Infrared Radiometer Sounder and the Stratospheric Aerosol and Gas Experiment II. *J. of Geophys. Res.*, **102** (29), 29,893-29,900.

Wylie, D. P., and W. P. Menzel, 1999: Eight years of high cloud statistics using HIRS. *J. Climate*, **12**, 170-184.